Defect-induced magnetism in graphene

Oleg V. Yazyev* and Lothar Helm
Ecole Polytechnique Fédérale de Lausanne (EPFL), Institute of Chemical Sciences and Engineering, CH-1015 Lausanne, Switzerland
(Received 21 January 2007; published 8 March 2007)

We study from first principles the magnetism in graphene induced by single carbon atom defects. For two types of defects considered in our study, the hydrogen chemisorption defect and the vacancy defect, the itinerant magnetism due to the defect-induced extended states has been observed. Calculated magnetic moments are equal to $1\mu_B$ per hydrogen chemisorption defect and $1.12-1.53\mu_B$ per vacancy defect depending on the defect concentration. The coupling between the magnetic moments is either ferromagnetic or antiferromagnetic, depending on whether the defects correspond to the same or to different hexagonal sublattices of the graphene lattice, respectively. The relevance of itinerant magnetism in graphene to the high-T_C magnetic ordering is discussed.

DOI: 10.1103/PhysRevB.75.125408 PACS number(s): 75.75.+a, 61.72.Ji, 71.15.−m, 81.05.Uw

I. INTRODUCTION

The last two decades were marked with the discoveries of new allotropic modifications of carbon and related nanostructures. Graphene, the single two-dimensional sheet of graphite, is the starting point for many carbon nanomaterials, which are commonly called nanographites. These materials, being diverse in atomic structure, display a wide range of electronic properties. Magnetism of carbon materials[1] is of particular interest since in current technological applications magnetic materials are based on d and f elements. New carbon-based magnetic materials would greatly extend the limits of technologies relying on magnetism. Even more promising is the application of such materials in the design of nanoscale magnetic and spin electronics devices.

While ideal graphite and carbon nanotubes are in itself nonmagnetic, experimental observations of magnetic ordering are often explained by the presence of impurities,[2] boundaries,[3,4] or defects.[5–8] Defects in nanographites[9] can be created intentionally by irradiating material with electrons or ions.[10–13] By manipulating the conditions of irradiation, it is possible to tune, in a flexible way, the properties of the carbon-based materials.[14–17] Examples of simple defects in nanographites are single-atom vacancies and hydrogen chemisorption defects. The former defect type is produced upon the irradiation with high-energy particles,[6] while the latter is the major outcome of the hydrogen plasma treatment.[10] The common feature of both types of defects is that only one carbon atom is removed from the π conjugation network of the graphene sheet. The single-atom defects on the graphene lattice give rise to quasilocalized states at the Fermi level.[10,18–20] The graphene lattice is the bipartite lattice. It can be viewed as two interpenetrating hexagonal sublattices of carbon atoms (labeled α and β). When a defect is created in the α lattice, only the p_z orbitals of carbon atoms in the β sublattice contribute to the quasilocalized state, and vice versa. These states extend over several nanometers around the defects forming characteristic $(\sqrt{3}\times\sqrt{3})R30^\circ$ superstructures recognized in scanning tunneling microscopy (STM) images. Analyzing the position and the orientation of the superstructures one can precisely locate the defect and determine the sublattice to which it belongs.[18,21] The fact that quasilocalized states lie at the Fermi level suggests that itinerant (Stoner) magnetism can be induced by the electron exchange instability. It has been argued recently that the Stoner ferromagnetism with high Curie temperatures T_C can be expected for sp electron systems.[22] On the other hand, the Ruderman-Kittel-Kasuya-Yoshida (RKKY) coupling[23] of localized magnetic moments in graphene is too weak to result in high T_C.[24] Another recent work has shown that the RKKY-type interactions in graphene are suppressed.[25]

In this work, we investigate, using first-principles approaches, the itinerant magnetism originating from the quasilocalized states induced by single-atom point defects in graphene. The results obtained can eventually be extended, with some precautions, to defects in other nanographites.

II. COMPUTATIONAL METHODS AND MODELS

The model system consists of a periodic two-dimensional superlattice of defects in graphene [Fig. 1(a)]. The supercell size can be varied resulting in different distances d between the neighbor defects on the superlattice and, thus, in different defect concentrations. The results can be further extrapolated to the cases of low defect concentrations. For the chosen supercell, the resulting distance between neighbor defects is about $3na_{cc}$, where $a_{cc}=1.42$ Å is the carbon-carbon distance in graphene. The corresponding number of carbon atoms per unit cell is $6n^2$. Our investigation is restricted to the cases with $n=2-6$. The largest system considered ($n=6$) is characterized by about 25 Å separation between neighbor defects, which corresponds to a defect concentration of 0.5%.

Density-functional theory calculations were performed using the SIESTA code.[26,27] The generalized gradient approximation exchange-correlation density functional of Perdew, Burke, and Ernzerhof[28] (PBE) was employed. All calculations were performed in the spin-unrestricted manner using the diagonalization-based method for solving Kohn-Sham equations. The shifted Monkhorst-Pack grids[29] corresponding to a cutoff of 100 Bohrs were used to sample the Brillouin zone in two dimensions. Atomic positions and cell dimensions were relaxed. The numerical atomic orbital basis set of single-ζ plus one polarization function (SZP) quality was used for the whole range of models studied. All calcu-

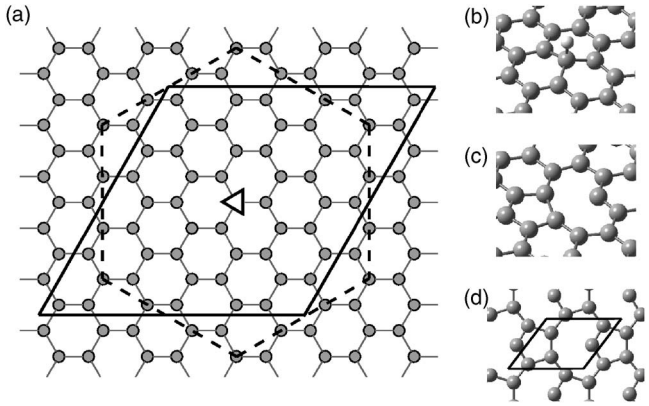

FIG. 1. (a) Definition of the extendable two-dimensional hexagonal lattice of defects in the graphene sheet. The unit cell and the Voronoi cell are shown as full and dashed lines, respectively. The defective atom is labeled by the triangle according to the orientation of the defect state $\sqrt{3}\times\sqrt{3}$ superstructure. The size of the supercell shown here corresponds to $9a_{cc}$ separation between neighbor defects ($n=3$). (b) Structure of the hydrogen chemisorption defect. (c) Structure of the vacancy defect. (d) Hexagonal closest packing ($n=1$) of vacancy defects with the corresponding unit cell.

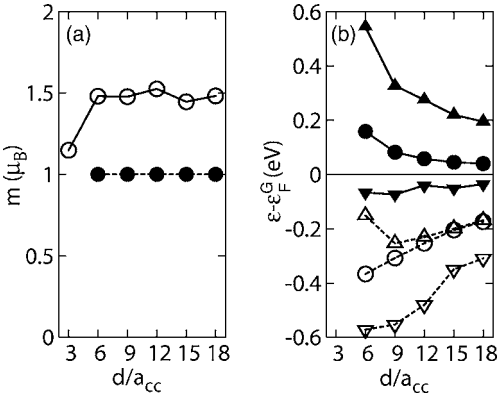

FIG. 2. (a) Calculated magnetic moment per defect vs the separation d between the neighbor hydrogen chemisorption defects (●) and the neighbor vacancy defects (○). (b) Fermi energies (●,○), majority spin (▲,△), and minority spin (▼,▽) band maxima versus the defect separation d for the hydrogen chemisorption defects (filled symbols), and the vacancy defects (open symbols). The Fermi level of ideal graphene is taken as zero.

lations for the models with $n=2-4$ were reproduced using the basis set of double-ζ plus one polarization function (DZP) quality. For all electronic structure quantities discussed in this study (magnetic moment, Fermi levels, and band maxima), there is good agreement between the results of the two basis sets, despite the slight overestimation of the C–C bond length found in the SZP calculations.

III. DISCUSSION OF RESULTS

In the following, we present our results for the two types of defects mentioned above. The structure of the hydrogen chemisorption defect is shown in Fig. 1(b). This defect is characterized by the slight protrusion of the hydrogenated carbon atom and the very small displacement of all other neighbor carbon atoms.[7,30] The single-atom vacancy defect in graphene is nearly planar [Fig. 1(c)]. The local threefold symmetry breaks down due to the Jahn-Teller distortion induced by the reconstruction of two dangling bonds left after removing the carbon atom. This gives rise to the in-plane displacement of other carbon atoms in the graphene lattice.[6,31] The third dangling bond is left unsaturated providing a contribution of magnitude $1\mu_B$ to the intrinsic magnetic moment of the defect. For the case of the vacancy-type defect [Fig. 1(d)] in the closest packing geometry ($n=1$) no single six-membered ring remains. This interesting structure can be considered as yet another hypothetical allotropic modification of carbon for which one may expect a high specific magnetic moment.

Magnetism induced by the presence of quasilocalized defect states $\psi_d(\vec{r})$ has been observed in the case of both defect types. The hydrogen chemisorption defect gives rise to the strong Stoner ferromagnetism[32] with a magnetic moment of $1\mu_B$ per defect at all studied concentrations [Fig. 2(a)]. The flat defect bands give rise to the very narrow peaks ($W<0.2$ eV), which are necessary for the stability of magnetic ordering at high temperatures.[22] The defect band maxima for the majority spin and the minority spin components lie, respectively, lower and higher than the Fermi levels for both defective and ideal graphene [Fig. 2(b)]. The hydrogen chemisorption motif is charge neutral and spin polarized in the wide range of defect concentrations. On the contrary, fractional magnetic moments and weak Stoner ferromagnetism[32] have been observed for the vacancy-type defect models. A magnetic moment of $1.15\mu_B$ has been predicted for the closest packing of vacancy type defects ($n=1$) [Fig. 1(d)], while for smaller defect concentrations the magnetic moment was found to vary in the range of $1.45-1.53\mu_B$ per defect [Fig. 2(a)]. For the vacancy-type defect, the total magnetic moment is determined by the contribution ($1\mu_B$) of the localized sp^2 dangling bond state (atom 1 in Fig. 4 and the contribution ($<1\mu_B$) of the extended defect state $\psi_d(\vec{r})$ (labeled p_z in Fig. 3).

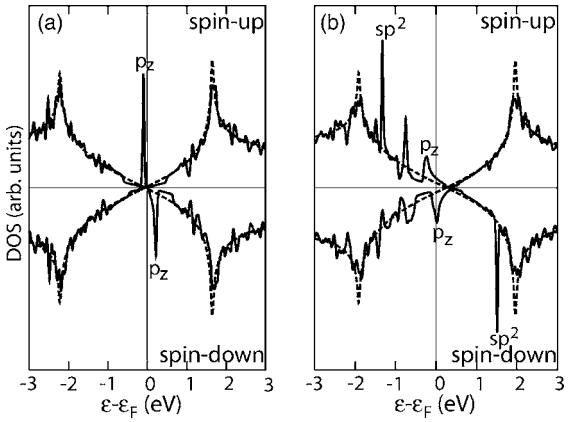

FIG. 3. Density of states plots for the systems with (a) the hydrogen chemisorption defects and with (b) the vacancy defects ($n=4$). The dashed line shows the density of states of the ideal graphene. Labels indicate the character of the defect states.

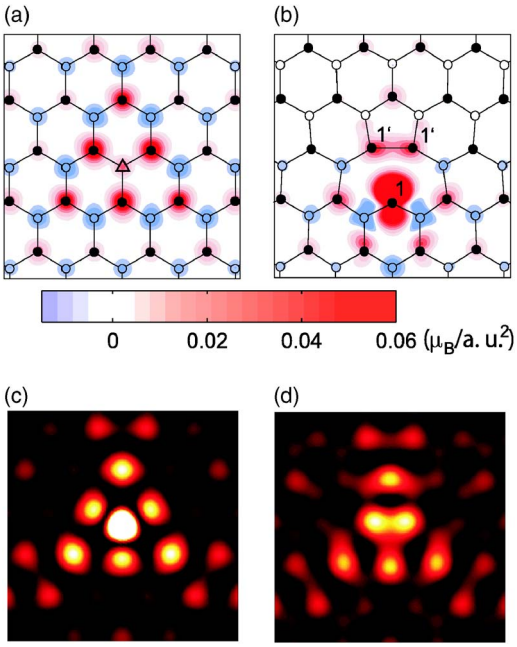

FIG. 4. (Color online) Spin-density projection (in μ_B/a.u.^{2}) on the graphene plane around (a) the hydrogen chemisorption defect (△) and (b) the vacancy defect in the α sublattice. Carbon atoms corresponding to the α sublattice (○) and to the β sublattice (●) are distinguished. Simulated STM images of the defects are shown in (c) and (d), respectively.

The width of the defect state bands and the overall modification of the band structure are larger in the case of the vacancy type defects [Fig. 3(b)]. The partial spin polarization of $\psi_d(\vec{r})$ (filled majority spin band and half-filled minority spin band) is explained by the self-doping [charge transfer from the bulk to $\psi_d(\vec{r})$], which arises from the stabilization of the defect state. The stabilization of vacancy defect extended states is possible in the case of a significant coupling between the second-nearest-neighbor atoms belonging to the same sublattice.[20] In the case of the vacancy defect, the indirect coupling is justified by the formation of the covalent bond between the two carbon atoms 1′ [Fig. 4(b)] that follows the defect reconstruction. No such bond is possible in the case of hydrogen chemisorption. Thus, the character of the defect-induced magnetism depends on the possibility of covalent bonding between the second-nearest-neighbor atoms due to the reconstruction. This provides an interesting opportunity for tailoring magnetic properties of materials.

The defect state exchange splitting, defined as the difference between the corresponding majority spin and minority spin band maxima, decreases as the defect concentration decreases. This is not surprising since the degree of the localization of the defect states depends on the defect concentration.[20] At the lowest studied defect concentration of 0.5%, the exchange splitting $d\epsilon_x$ were found to be 0.23 and 0.14 eV for the hydrogen chemisorption and vacancy defects, respectively. In the latter case, the splitting is smaller due to the partial spin polarization of the defect band. Since in both cases $d\epsilon_x > k_B T$ for $T \approx 300$ K, the Stoner theory predicts T_C above room temperature for defect concentrations of the order of 1%. The decrease of the Stoner theory T_C due to spin-wave excitations is expected to be ineffective for the case of carbon-based materials.[22] At low concentrations, the magnetism in defective nanographites is expected to be sensitive to the variations of the Fermi energy resulting from self-doping, to the presence of other defects or applied bias, and to the disorder-induced broadening.

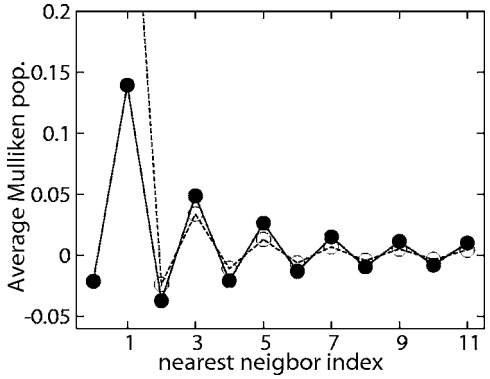

FIG. 5. Dependence of the spin populations averaged over ith nearest neighbors of the hydrogen chemisorption defects (●) and the vacancy defects (○). The spin population for the first-nearest-neighbor atoms of the vacancy defect (0.39) are out of scale due to the contribution of the localized sp^2 dangling-bond state.

The distributions of the electron spin magnetization density in the vicinity of both types of defects clearly show the characteristic $\sqrt{3}\times\sqrt{3}$ patterns also observed for the charge density in the STM experiments. For the hydrogen chemisorption defect the projection of the spin density [Fig. 4(a)] on the graphene plane clearly shows threefold symmetry. For the vacancy-type defect, the symmetry is broken due to the Jahn-Teller distortion [Fig. 4(b)]. The localized magnetic moment associated with the dangling bond of atom 1 can also be observed. The simulated STM images [Figs. 4(c) and 4(d)] based on our calculations agree with experimental observations.[10,18,19] The distribution of the electron spin density is represented in Fig. 5 ($n=6$ model) by means of the Mulliken spin populations averaged over ith nearest neighbors to the defect atom. The spin populations show a damped oscillation behavior as a function of the nearest-neighbor index and, therefore, of the distance to the defect. The magnetization pattern is explained by the fact that the defect state is distributed over the sites of the sublattice complementary to the one in which the defect was created (i.e., over the odd nearest neighbors), and shows a power law decay.[20] The major positive contribution to the electron spin density is defined by the exchange splitting of the defect states. In addition, the exchange spin-polarization effect (i.e., the response of the fully populated valence bands to the magnetization of the defect states) results in a negative spin density on the even-nearest-neighbor sites and in the enhancement of a positive spin density on the odd-nearest-neighbor sites (see Fig. 4). A similar phenomenon takes place in the case of the neutral bond-length alternation defect states (neutral solitons) in one-dimensional polyene chains.[33,34] The calculated magnitude of the negative spin-polarization is $\approx 1/3$ of the positive spin populations on the neighbor sites in the vicinity of the defect site. This is close to the ratio observed for the *trans*-polyacetylene.[33] The magnitudes of the spin popula-

tions are lower in the case of the vacancy defect because of the fractional spin polarization of the defect band.

According to the Stoner picture, the magnetic ordering is driven by the exchange energy $E_x \sim -\Sigma_i M_j^2$, with M_j being the magnetization of the p_z orbital of the jth carbon atom.[32] Ferromagnetic ordering is the only possibility for the magnetism originating from quasilocalized states induced by defects in the same sublattice because of the nonoscillating behavior of both (i) M_j within the same sublattice and (ii) the indirect (RKKY) coupling due to the semimetallic properties of graphene.[24] On the contrary, for the case of defect states in different sublattices, E_x is minimized when the coupling is antiferromagnetic. In this case, the mechanism of the exchange coupling is defined by the indirect spin-polarization effect. The strength of the coupling between the defect-induced magnetic moments located in different sublattices depends on the defect concentration since $E_x \sim -\Sigma_i M_j^2$. The contribution of the magnetic moment associated with a single defect is $\Sigma_i M_j^2 \sim \Sigma_j |\psi_d(\vec{r}_j)|^4 \sim \log^{-2}(N)$, where $1/N$ is the defect concentration.[20] To further illustrate this point, we calculated the ground-state magnetic configuration of the system with three close hydrogen chemisorption defects using the density-functional theory (DFT) approach. We found that in the ground-state configuration, two defects in the α sublattice are coupled ferromagnetically with each other and antiferromagnetically with the third defect in the β sublattice (Fig. 6). The resulting magnetic moment of this system amounts to $2-1=1\mu_B$ in agreement with the second Lieb theorem,[35] and the characteristic $\sqrt{3}\times\sqrt{3}$ patterns of the magnetization density associated with individual defects can be recognized. In nanographite materials with defects present with an equal probability in both sublattices, the overall correlation of the magnetic moments is expected to be antiferromagnetic. The antiferromagnetic ordering was experimentally observed in carbon nanohorns.[36,37]

In addition, we found that the proton spin of chemisorption hydrogen atom shows a strong magnetic coupling to the electron in the quasilocalized defect state. Even for the lowest defect concentration studied, we find the magnitude of Fermi contact hyperfine interaction of ≈35 G. One can consider the nuclear spin quantum computer implementation originally proposed by Kane[38] based on carbon nanostructures.

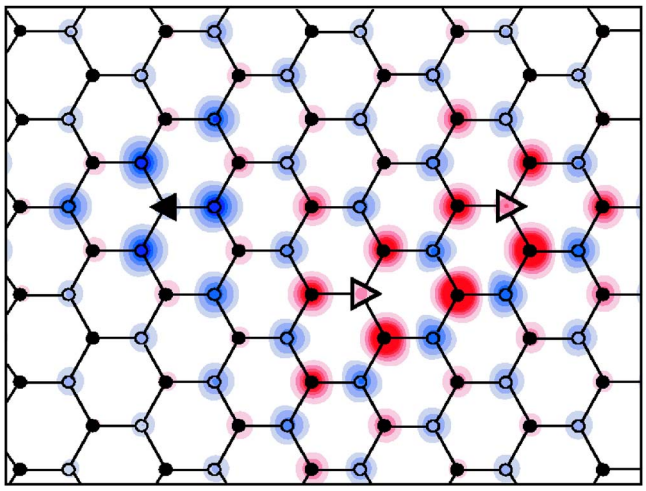

FIG. 6. (Color online) Spin density distribution in the system with three hydrogen chemisorption defects [two defects in sublattice α (▷) and one in sublattice β (◀)]. The same scale as in Fig. 4 applies.

IV. CONCLUSIONS

In conclusion, our calculations reveal the itinerant magnetism triggered by simple defects in graphene and stable over the wide range of concentrations. It is notable that the itinerant magnetism does not require the presence of highly reactive unsaturated dangling bonds. Both ferromagnetic and antiferromagnetic scenarios of the magnetic correlation are possible with the second being more probable for truly disordered systems. The reconstruction of vacancy defects was found to be responsible for the partial suppression of magnetic moments and for the broadening of defect bands. We argue that the defect-induced itinerant magnetism is responsible for the experimentally observed high-T_C ferromagnetism of irradiated graphite samples.

ACKNOWLEDGMENTS

The authors acknowledge G. Buchs, D. Ivanov, M. I. Katsnelson, and I. Tavernelli for discussions. O.V.Y. thanks the Swiss National Science Foundation for financial support. The computational resources were provided by the Swiss Center for Scientific Computing and the DIT-EPFL.

*Electronic address: oleg.yazyev@epfl.ch

[1] *Carbon-Based Magnetism: An Overview of Metal Free Carbon-Based Compounds and Materials*, edited by T. Makarova and F. Palacio (Elsevier, Amsterdam, 2005).
[2] J. M. D. Coey, M. Venkatesan, C. B. Fitzgerald, A. P. Douvalis, and I. S. Sanders, Nature (London) **420**, 156 (2002).
[3] H. Lee, Y.-W. Son, N. Park, S. Han, and J. Yu, Phys. Rev. B **72**, 174431 (2005).
[4] S. Okada and A. Oshiyama, Phys. Rev. Lett. **87**, 146803 (2001).
[5] Y.-H. Kim, J. Choi, K. J. Chang, and D. Tománek, Phys. Rev. B **68**, 125420 (2003).
[6] P. O. Lehtinen, A. S. Foster, Y. Ma, A. V. Krasheninnikov, and R. M. Nieminen, Phys. Rev. Lett. **93**, 187202 (2004).
[7] E. J. Duplock, M. Scheffler, and P. J. D. Lindan, Phys. Rev. Lett. **92**, 225502 (2004).
[8] J. M. Carlsson and M. Scheffler, Phys. Rev. Lett. **96**, 046806 (2006).
[9] J.-C. Charlier, Acc. Chem. Res. **35**, 1063 (2002).
[10] P. Ruffieux, O. Gröning, P. Schwaller, L. Schlapbach, and P. Gröning, Phys. Rev. Lett. **84**, 4910 (2000).

[11] P. Esquinazi, D. Spemann, R. Höhne, A. Setzer, K.-H. Han, and T. Butz, Phys. Rev. Lett. **91**, 227201 (2003).
[12] A. Hashimoto, K. Suenaga, A. Gloter, K. Urita, and S. Iijima, Nature (London) **430**, 870 (2004).
[13] K. Urita, K. Suenaga, T. Sugai, H. Shinohara, and S. Iijima, Phys. Rev. Lett. **94**, 155502 (2005).
[14] F. Banhart, Rep. Prog. Phys. **62**, 1181 (1999).
[15] C. Mikó, M. Milas, J. W. Seo, E. Couteau, N. Barisic, R. Gaál, and L. Forró, Appl. Phys. Lett. **83**, 4622 (2003).
[16] K.-H. Han, D. Stepmann, P. Esquinazi, R. Höhne, V. Riede, and T. Butz, Adv. Mater. (Weinheim, Ger.) **15**, 1719 (2003).
[17] A. Kis, G. Csányi, J.-P. Salvetat, T.-N. Lee, E. Couteau, A. J. Kulik, W. Benoit, J. Brugger, and L. Forró, Nat. Mater. **3**, 153 (2004).
[18] H. A. Mizes and J. S. Foster, Science **244**, 559 (1989).
[19] P. Ruffieux, M. Melle-Franco, O. Gröning, M. Bielmann, F. Zerbetto, and P. Gröning, Phys. Rev. B **71**, 153403 (2005).
[20] V. M. Pereira, F. Guinea, J. M. B. Lopes dos Santos, N. M. R. Peres, and A. H. Castro Neto, Phys. Rev. Lett. **96**, 036801 (2006).
[21] K. Kelly and N. Halas, Surf. Sci. **416**, L1085 (1998).
[22] D. M. Edwards and M. I. Katsnelson, J. Phys.: Condens. Matter **18**, 7209 (2006).
[23] M. A. Rudermann and C. Kittel, Phys. Rev. **96**, 99 (1954); T. Kasuya, Prog. Theor. Phys. **16**, 45 (1965); K. Yoshida, Phys. Rev. **106**, 893 (1958).
[24] M. A. H. Vozmediano, M. P. López-Sancho, T. Stauber, and F. Guinea, Phys. Rev. B **72**, 155121 (2005).
[25] V. K. Dugaev, V. I. Litvinov, and J. Barnas, Phys. Rev. B **74**, 224438 (2006).
[26] E. Artacho, J. D. Gale, A. García, J. Junquera, R. M. Martin, P. Ordejón, D. Sánchez-Portal, and J. M. Soler, SIESTA, Version 1.3, 2004.
[27] J. M. Soler, E. Artacho, J. D. Gale, A. García, J. Junquera, P. Ordejón, and D. Sánchez-Portal, J. Phys.: Condens. Matter **14**, 2745 (2002).
[28] J. P. Perdew, K. Burke, and M. Ernzerhof, Phys. Rev. Lett. **77**, 3865 (1996).
[29] H. J. Monkhorst and J. D. Pack, Phys. Rev. B **13**, 5188 (1976).
[30] P. Ruffieux, O. Gröning, M. Bielmann, P. Mauron, L. Schlapbach, and P. Gröning, Phys. Rev. B **66**, 245416 (2002).
[31] A. J. Lu and B. C. Pan, Phys. Rev. Lett. **92**, 105504 (2004).
[32] P. Mohn, *Magnetism in the Solid State* (Springer-Verlag, Berlin, 2003).
[33] H. Thomann, L. R. Dalton, Y. Tomkiewicz, N. S. Shiren, and T. C. Clarke, Phys. Rev. Lett. **50**, 533 (1983).
[34] B. Kirtman, M. Hasan, and D. M. Chipman, J. Chem. Phys. **95**, 7698 (1991).
[35] E. H. Lieb, Phys. Rev. Lett. **62**, 1201 (1989); Phys. Rev. Lett. **62**, 1927(E) (1989).
[36] S. Garaj, L. Thien-Nga, R. Gaal, L. Forró, K. Takahashi, F. Kokai, M. Yudasaka, and S. Iijima, Phys. Rev. B **62**, 17115 (2000).
[37] H. Imai, P. K. Babu, E. Oldfield, A. Wieckowski, D. Kasuya, T. Azami, Y. Shimakawa, M. Yudasaka, Y. Kubo, and S. Iijima, Phys. Rev. B **73**, 125405 (2006).
[38] B. E. Kane, Nature (London) **393**, 133 (1998).